POLITECNICO DI TORINO
Repository ISTITUZIONALE

Diagnostic of fast-ion energy spectra and densities in magnetized plasmas

(Article begins on next page)

Diagnostic of fast-ion energy spectra and densities in magnetized plasmas

M. Salewski, [a,1] **M. Nocente,** [b,c] **B. Madsen,** [a] **I. Abramovic,** [d] **G. Gorini,** [b,c] **A.S. Jacobsen,** [e] **V.G. Kiptily,** [e] **S.B. Korsholm,** [a] **D. Moseev,** [d] **S.K. Nielsen,** [a] **A.F.L. Poulsen** [a] **J. Rasmussen,** [a] **M. Tardocchi,** [c] **B. Geiger,** [f] **J. Eriksson,** [g] **the JET Contributors,** [2] **the ASDEX Upgrade Team, and the EUROfusion MST1 Team** [3]

[a] *Technical University of Denmark, Kgs. Lyngby, Denmark*

[b] *Department of Physics, University of Milano Bicocca, Milano, Italy*

[c] *Istituto di Fisica del Plasma, Consiglio Nazionale delle Ricerche, Milano, Italy*

[d] *Max-Planck-Institut für Plasmaphysik, Greifswald, Germany*

[e] *CCFE, Culham Science Centre, Abingdon, Oxon, United Kingdom*

[f] *Max-Planck-Institut für Plasmaphysik, Garching, Germany*

[g] *Department of Physics and Astronomy, Uppsala University, Sweden*

E-mail: msal@dtu.dk

ABSTRACT: The measurement of the energy spectra and densities of α-particles and other fast ions are part of the ITER measurement requirements, highlighting the importance of energy-resolved energetic-particle measurements for the mission of ITER. However, it has been found in recent years that the velocity-space interrogation regions of the foreseen energetic-particle diagnostics do not allow these measurements directly. We will demonstrate this for γ-ray spectroscopy (GRS), collective Thomson scattering (CTS), neutron emission spectroscopy and fast-ion D_α spectroscopy by invoking energy and momentum conservation in each case, highlighting analogies and differences between the different diagnostic velocity-space sensitivities. Nevertheless, energy spectra and densities can be inferred by velocity-space tomography which we demonstrate using measurements at JET and ASDEX Upgrade. The measured energy spectra agree well with corresponding simulations. At ITER, α-particle energy spectra and densities can be inferred for energies larger than 1.7 MeV by velocity-space tomography based on GRS and CTS. Further, assuming isotropy of the α-particles in velocity space, their energy spectra and densities can be inferred by 1D inversion of spectral single-detector measurements down to about 300 keV by CTS. The α-particle density can also be found by fitting a model to the CTS measurements assuming the α-particle distribution to be an isotropic slowing-down distribution.

KEYWORDS: Nuclear instruments and methods for hot plasma diagnostics, Computerized Tomography (CT)

---

[1]Corresponding author.
[2]See author list of X. Litaudon et al 2017 Nucl. Fusion **57** 102001
[3]See author list of H. Meyer et al 2017 Nucl. Fusion **57** 102014

Contents

1 Introduction

Measurements of the densities and energy spectra of α-particles and other fast ions in ITER are considered highly important and constitute the ITER measurement requirements for energetic particle diagnostics [1]. However, in recent years it was found that the spectra measurable by common fast-ion diagnostics are sensitive to restricted yet rather broad regions in phase space such that densities and energy spectra cannot be directly measured by individual diagnostics. This is illustrated by so-called weight functions [2–12]. Examples of weight functions for neutron emission spectrometry (NES), γ-ray spectrometry (GRS), collective Thomson scattering (CTS) and fast-ion D_α (FIDA) spectroscopy are presented in figure 1. The 2D velocity space in figure 1 is described by the energy E and the pitch $p = v_\parallel/v$ where $v_\parallel$ is the velocity component along the magnetic field and v is the speed. Each point in a measured spectrum is sensitive to a particular region in 2D velocity space such as those illustrated in red in figure 1. We also illustrate a hypothetical weight function which would allow direct energy resolution. One-step reaction GRS [13] is the only diagnostic with some direct energy resolution [7]. The shapes of weight functions for these diagnostics will be explained in this paper by invoking energy and momentum conservation.

Despite the restricted velocity-space coverage of individual measurements, energy spectra and densities can still be found by solving an inverse problem to infer the fast-ion 2D velocity distribution function from the combined set of available measurements. This is referred to as velocity-space tomography [11, 12, 14–29]. Integration over the pitch gives the energy spectrum [20], and subsequent integration over the energy gives the density [18, 22]. If we assume isotropy in velocity space, we can use this approach to also invert measurements from only one detector [28]. Whereas velocity-space tomography is the only known way to measure energetic-particle energy spectra, the energetic-particle density can also be inferred by fitting spectra to the measurements assuming a functional form of the velocity distribution function, e.g. a slowing-down distribution.

This paper consists of two main parts. Firstly, we will show that the velocity-space interrogation regions of fast-ion diagnostics are a consequence of energy and momentum conservation. We will

consider one-step reaction GRS, NES, FIDA (or generally charge-exchange recombination spectroscopy (CXRS)) and CTS as well as the analogous electron diagnostic Thomson scattering (TS). Secondly, we will demonstrate techniques to measure energy spectra by velocity-space tomography and related data inversion techniques using measurements at ASDEX Upgrade and JET as well as modelling for ITER.
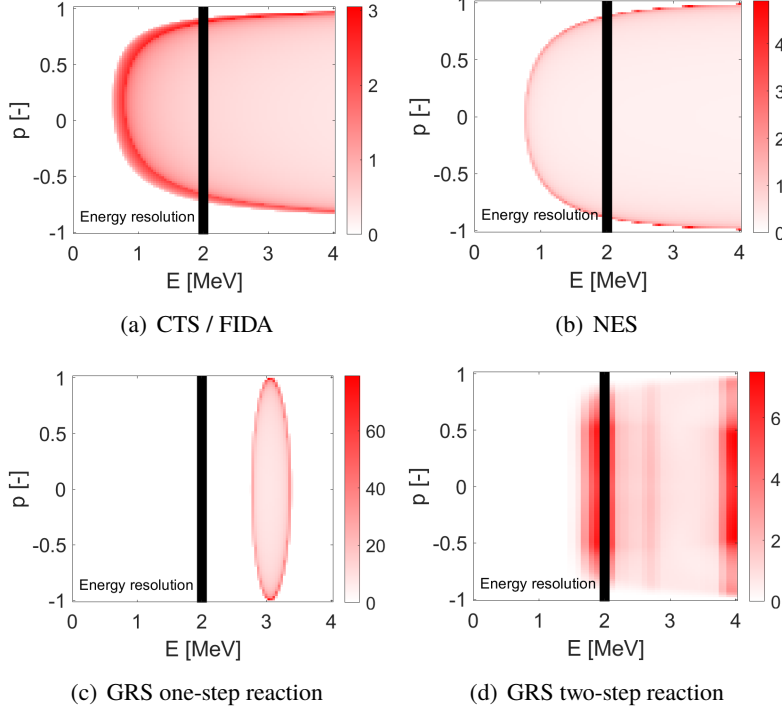

Figure 1. Examples of weight functions [a.u.] of various fast-ion diagnostics illustrated in red as compared to the form required by a weight function to achieve direct energy resolution, marked by a black line at 2 MeV.

2 Velocity-space interrogation regions

Energy and momentum conservation determine to which velocity-space regions energetic-particle diagnostics are sensitive. These conservation principles relate the energy and momentum of the energetic particle in the plasma to the energy and momentum of the detectable particle (including photons). This is well-established for NES and GRS weight functions [5, 7, 8, 17]. FIDA and CTS as well as the related diagnostics CXRS and TS exploit the Doppler shift. The Doppler shift is in turn implied by energy and momentum conservation [30]. Hence we invoke energy and momentum conservation for each diagnostic and derive the shape of weight functions from these principles. This common framework highlights reasons for analogies and differences among the weight functions. To focus on the large-scale shapes of the observable velocity-space regions, we here neglect effects leading to small changes in the observable velocity space, such as non-zero plasma temperatures, Stark splitting or instrumental broadening [4, 5, 7, 17]. We do not consider any reaction probabilities since they influence only the amplitudes of the weight functions but not the shapes [4, 5, 7, 17].

The following sections will show that, for each diagnostic, the fast-ion velocity component u along the line-of-sight appears when the momentum and energy equations are combined. u is related to the energy E_d of the detectable particle (including photons) by these conservation principles. u is also related to the gyroangle Γ of the energetic particle according to [3]

$$u = v_\parallel \cos \phi + v_\perp \sin \phi \cos \Gamma \tag{2.1}$$

where ϕ is the observation angle between the line-of-sight and the magnetic field and $v_\perp$ is the velocity component perpendicular to the magnetic field. Given u, ϕ and $(v_\parallel, v_\perp)$, the corresponding gyroangles can be computed. The resulting probability that the detected particle has energies in the interval $[E_{d,1}, E_{d,2}]$ can be related to the probability that the fast ion has a line-of-sight velocity in the interval $[u_1, u_2]$ (see next section) and to the corresponding fraction of the gyroorbit [4]:

$$\text{prob}(E_{d,1} < E_d < E_{d,2}|\phi, v_\parallel, v_\perp) = \text{prob}(u_1 < u < u_2|\phi, v_\parallel, v_\perp)$$
$$= \frac{\Gamma_1 - \Gamma_2}{\pi} = \frac{1}{\pi} \left(\arccos \frac{u_1 - v_\parallel \cos \phi}{v_\perp \sin \phi} - \arccos \frac{u_2 - v_\parallel \cos \phi}{v_\perp \sin \phi} \right). \tag{2.2}$$

The conditioning sign '|' means 'given'. The unobserved velocity space corresponds to a probability of zero such that no gyroangle exists allowing a detection in the interval $[E_{d,1}, E_{d,2}]$. The observed velocity space corresponds to probabilities between zero and one. In this case a detection in the interval $[E_{d,1}, E_{d,2}]$ is possible on some parts of the gyroorbit (for prob=1 on the full orbit). Equation 2.2 shows how to find the observable velocity space from the line-of-sight velocity u for the diagnostics that we consider. In the following we will calculate u from the energy E_d and momentum p_d of the detected particle for each diagnostic using energy and momentum conservation.

3   Energy and momemtum conservation principles for fast-ion diagnostics

We first formulate the specific non-relativistic energy and momentum conservation equations for NES, GRS, FIDA, CXRS, CTS and TS that connect the projected velocities u with the velocities of the detected particles (including photons). In the second step we will solve a set of generic conservation equations modelling all of these fast-ion diagnostics.

GRS and NES:
Consider a generic one-step fusion reaction between a fast particle (f) and a reactant thermal particle (r) to form a reaction product (pr) releasing a detectable photon or a neutron (d). The non-relativistic energy and momentum conservation equations for particles with mass m, velocity $\mathbf{v}$ and $v = |\mathbf{v}|$ are, respectively,

$$\frac{1}{2}m_f v_f^2 + \frac{1}{2}m_r v_r^2 + Q = \frac{1}{2}m_{pr} v_{pr}^2 + E_d, \tag{3.1}$$
$$m_f \mathbf{v}_f + m_r \mathbf{v}_r = m_{pr} \mathbf{v}_{pr} + \mathbf{p}_d. \tag{3.2}$$

Here Q is the released energy, and E_d and $\mathbf{p}_d$ are the energy and momentum of the emitted detected particle (or photon), respectively.

FIDA and CXRS:

Usually FIDA weight functions are calculated invoking the Doppler shift. Here we instead invoke energy and momentum conservation which in turn imply the Doppler shift [30]. In the rest frame of the excited atom, the energy of the released photon, Q, is the difference between the energy levels U and U' before and after the emission, respectively: $Q = U - U' = h f_0$ where h is Planck's constant and f_0 is the frequency. Primes (') mark quantities after the reaction. In the lab frame the total energy is the sum of the kinetic energy and the energy level U. Energy and momentum conservation of the D_α-emission process in the lab frame are then [30]

$$\frac{1}{2}m_f v_f^2 + U = \frac{1}{2}m_f v_f'^2 + U' + E_d, \tag{3.3}$$

$$m_f \mathbf{v}_f = m_f \mathbf{v}_f' + \mathbf{p}_d. \tag{3.4}$$

CTS and TS:

Whereas TS measures the distribution of electrons in the plasma, CTS measures the distribution of ions. Scattering off ions is negligible compared with scattering off electrons due to the large proton-to-electron mass ratio $m_p/m_e = 1836$. The difference between TS and CTS can be illustrated using the dressed particle model which is a simplification of a rigorous kinetic treatment. The dressed particle model is well-suited to highlight the analogy between CTS and TS and, together with energy and momentum conservation, also with other fast-ion diagnostics. A test charge in a plasma is surrounded by other charges that screen the potential of the test charge. The size of this screening cloud is on the order of the Debye length λ_D. A test particle together with its screening cloud is referred to as a dressed particle. For example, the screening cloud of an ion is composed of (a surplus of) electrons and (a lack of) ions. We consider very fast ions so that thermal ions are too slow to participate strongly in the screening, and hence the screening cloud consists mostly of electrons.

In incoherent Thomson scattering, the wavelength of the fluctuation wave field is much smaller than the Debye length, so that scattering occurs incoherently at random phases of the wave electric field. The scattering power due to individual electrons can then be summed to obtain the power due to Thomson scattering from a plasma. Hence we can consider energy and momentum conservation for an individual electron and incident (index i) and scattered (index s) photons,

$$\hbar\omega_i + \frac{1}{2}m_e v^2 = \hbar\omega_s + \frac{1}{2}m_e v'^2, \tag{3.5}$$

$$\hbar\mathbf{k}_i + m_e\mathbf{v} = \hbar\mathbf{k}_s + m_e\mathbf{v}', \tag{3.6}$$

where $\hbar = h/2\pi$, ω is the angular frequency, and $\mathbf{k}$ is the wave vector.

For CTS in the dressed particle model, the radiation is scattered off electrons in the screening cloud surrounding ions. As the wavelength of the mainly ion-induced fluctuation wave field is much larger than the Debye length, the phases of the fluctuation wave field of the test charge and the electrons in the screening cloud are correlated. Scattering from a test electron is therefore balanced by a lack of scattering from its screening cloud, and hence the electron signature in the detectable spectra is strongly suppressed. This cancellation does not occur for the comparatively immobile

ions which are therefore revealed by coherent or collective scattering from their screening clouds. Following the dressed particle model, the energy and momentum equations are identical with those for incoherent Thomson scattering with $m_e \rightarrow m_{di}$, where $m_{di} \approx m_i$ is the dressed ion mass which is about the same as the ion mass.

4 Generic energy and momentum equations for NES, GRS, CXRS, FIDA, TS and CTS

We can now formulate non-relativistic energy and momentum equations which conveniently encompass all of the above emission processes. These energy and momentum equations have in common that the energetic particle with energy $\frac{1}{2}m_f v_f^2$ and momentum $m_f \mathbf{v}_f$ undergoes a process in which a detectable particle with energy E_d and momentum $\mathbf{p}_d$ is formed. The detected particle may be a photon. In NES, GRS and CTS, the process involves another reactant with energy E_r and momentum $\mathbf{p}_r$, whereas for FIDA we will just set these to zero. Apart from the detectable particle, another particle with mass carries the energy $\frac{1}{2}m_{pr} v_{pr}^2$ and momentum $m_{pr} \mathbf{v}_{pr}$ for all processes. However, for CTS and FIDA $m_{pr} = m_f$ in a non-relativistic treatment. Lastly, there may be a change of the excitation states releasing an energy $Q = U - U'$ in the rest frame. Thus we get the non-relativistic energy and momentum equations in the lab frame:

$$\frac{1}{2}m_f v_f^2 + E_r + U = \frac{1}{2}m_{pr} v_{pr}^2 + U' + E_d, \tag{4.1}$$

$$m_f \mathbf{v}_f + \mathbf{p}_r = m_{pr} \mathbf{v}_{pr} + \mathbf{p}_d. \tag{4.2}$$

To solve these, we eliminate v_{pr} in the energy equation using the momentum equation:

$$\frac{1}{2}m_f v_f^2 + E_r + U = \frac{m_f^2}{2m_{pr}} v_f^2 - \frac{m_f}{m_{pr}} \mathbf{v}_f \cdot (\mathbf{p}_d - \mathbf{p}_r) + \frac{1}{2m_{pr}} (\mathbf{p}_d - \mathbf{p}_r)^2 + U' + E_d. \tag{4.3}$$

The fast-ion velocity appears in direction-independent terms as $v_f^2 = v_\parallel^2 + v_\perp^2$ and in the direction-dependent dot products including $\mathbf{v}_f$. The projection of the energetic particle velocity onto the momentum vector of the detectable particle, $\mathbf{v}_f \cdot \mathbf{p}_d$, highlights the selective role of the geometry of the line-of-sight. We solve for $\mathbf{v}_f \cdot (\mathbf{p}_d - \mathbf{p}_r)$ and set the difference in internal energies to $Q = U - U'$:

$$\mathbf{v}_f \cdot (\mathbf{p}_d - \mathbf{p}_r) = \frac{m_f - m_{pr}}{2} (v_\parallel^2 + v_\perp^2) + \frac{m_{pr}}{m_f} (E_d - E_r - Q) + \frac{(\mathbf{p}_d - \mathbf{p}_r)^2}{2m_f}. \tag{4.4}$$

Equation 4.4 is valid for all diagnostics that we consider. For NES and GRS, we neglect the energy and momentum of the thermal species ($v_f \gg v_r$). They are routinely taken into account in numeric weight function computations using the GENESIS code. For FIDA, these terms are not relevant and we consequently set them to zero.

The projected velocity onto the line-of-sight appears in the dot product $\mathbf{v}_f \cdot \mathbf{p}_d = u p_d$ where p_d is the magnitude of $\mathbf{p}_d$. Thus we get a simplified equation for the projected velocity u for NES, GRS and FIDA:

$$u = \frac{m_f - m_{pr}}{2p_d} (v_\parallel^2 + v_\perp^2) + \frac{m_{pr}}{m_f} \frac{E_d - Q}{p_d} + \frac{p_d}{2m_f}. \tag{4.5}$$

For NES, the detected particle is a neutron with $E_d = \frac{1}{2}m_n v_n^2$ and $p_d = m_n v_n$:

$$u_{NES} = \frac{m_f - m_{pr}}{2m_n v_n}(v_\parallel^2 + v_\perp^2) + \frac{m_{pr}}{m_f}\frac{\frac{1}{2}m_n v_n^2 - Q}{m_n v_n} + \frac{m_n v_n}{2m_f}. \tag{4.6}$$

This is the result obtained in reference [5]. Substitution of equation 4.6 into equation 2.2 reveals the velocity space interrogated by NES.

For GRS, the detected particle is a γ-ray with $E_d = E_\gamma$ and $p_d = E_\gamma/c$ where c is the speed of light:

$$u_{GRS} = c\left(\frac{m_f - m_{pr}}{2E_\gamma}(v_\parallel^2 + v_\perp^2) + \frac{m_{pr}}{m_f}\frac{E_\gamma - Q}{E_\gamma} + \frac{E_\gamma}{2m_f c^2}\right) \approx c\left(\frac{m_f - m_{pr}}{2E_\gamma}(v_\parallel^2 + v_\perp^2) + \frac{m_{pr}}{m_f}\frac{E_\gamma - Q}{E_\gamma}\right). \tag{4.7}$$

This is the result obtained in reference [7]. Substitution of equation 4.7 into equation 2.2 reveals the velocity space interrogated by GRS. A difference between the neutron and γ-ray spectrometry equations is that the last term is negligible for the γ-ray diagnostic as it is smaller by a factor of the order of the ratio of the energy of the γ and the rest energy of the ion.

Similar to GRS, FIDA relies on the emission of a photon. Hence we obtain basically the same equation for FIDA as for γ-rays. However, for FIDA we can set $m_{pr} = m_f$. We also set $E = hf$, $Q = hf_0$ and $p_d = hf/c$:

$$u_{FIDA} = c\left(\frac{f - f_0}{f} + \frac{hf}{2m_f c^2}\right) \approx c\left(\frac{f - f_0}{f}\right) = c\left(\frac{\lambda_0 - \lambda}{\lambda_0}\right). \tag{4.8}$$

Neglecting the second term containing the small ratio of the photon energy and the rest energy of the fast ion ($hf/m_f c^2 \sim 10^{-9}$), we obtain the usual Doppler shift formula determining the large-scale shape of FIDA weight functions which can be substituted into equation 2.2 to obtain the interrogated velocity space.

The analogy of the line-of-sight velocities obtained for FIDA (equation 4.8) and GRS (equation 4.7) becomes clear. The first term in equation 4.7 is quadratic in $v_\parallel$ and $v_\perp$ resulting in the circular shapes of one-step reaction GRS weight functions in $(v_\parallel, v_\perp)$-space. It drops out for $m_{pr} = m_f$ so that no circular shapes appear in Doppler-shift based weight functions (for the classical treatment). The second term in equation 4.7 is related to the Doppler shift. This term has a prefactor m_{pr}/m_f for GRS. For the usual Doppler shift as in FIDA, we have $m_{pr} = m_f$, whereas $m_{pr} \neq m_f$ describes the recoil due to the emission of the energetic γ-ray. The third term in equation 4.6 is important for NES only but is negligible for GRS and FIDA.

For CTS, consider first the generic equation 4.4. Introducing the energies and momenta of the incident photon (i) and the scattered photon (s), we set

$$\mathbf{p}_d = \hbar\mathbf{k}_s, \qquad \mathbf{p}_r = \hbar\mathbf{k}_i, \qquad E_d = \hbar\omega_s, \qquad E_r = \hbar\omega_i. \tag{4.9}$$

As the ion mass and the internal energies are not changed, we have $m_{pr} = m_f$ and $Q = 0$. Equation 4.4 simplifies to

$$\mathbf{v}_f \cdot (\mathbf{k}_s - \mathbf{k}_i) = \omega_s - \omega_i + \frac{\hbar(\mathbf{k}_s - \mathbf{k}_i)^2}{2m_f}. \tag{4.10}$$

We also introduce the differences (δ) of the frequencies and wavevectors of the incident photon (i) and the scattered photon (s),

$$\mathbf{k}_\delta = \mathbf{k}_s - \mathbf{k}_i, \qquad \omega_\delta = \omega_s - \omega_i, \tag{4.11}$$

and recover the Doppler shift relation for TS and CTS

$$\omega_\delta = \mathbf{v}_f \cdot \mathbf{k}_\delta - \frac{\hbar k_\delta^2}{2m_f}. \tag{4.12}$$

With $\mathbf{v}_f \cdot \mathbf{k}_\delta = u k_\delta$ we obtain

$$u_{CTS} = \frac{\omega_\delta}{k_\delta} + \frac{\hbar k_\delta}{2m_f}, \tag{4.13}$$

where the second term can be neglected. Equation 4.13 describes two Doppler shifts as apparent from equation 4.10: $\mathbf{v}_f \cdot \mathbf{k}_i$ and $\mathbf{v}_f \cdot \mathbf{k}_s$. The probe radiation has a Doppler shifted frequency in the rest frame of the particle and the emitted radiation from the moving particle has yet another Doppler-shifted frequency in the lab frame. The observable velocity-space for a CTS measurement is found by substitution of equation 4.13 into equation 2.2.

Electrons in hot plasmas have large speeds, often a significant fraction of the speed of light, so that a relativistic description may sometimes be necessary. The relativistic energy and momentum equations for CTS are

$$\hbar\omega_i + \gamma_f m_f c^2 = \hbar\omega_s + \gamma_f' m_f c^2, \tag{4.14}$$
$$\hbar\mathbf{k}_i + \gamma_f m_f \mathbf{v}_f = \hbar\mathbf{k}_s + \gamma_f' m_f \mathbf{v}_f', \tag{4.15}$$

containing the Lorentz factor γ_e with $\gamma_e^2 = 1/(1 - v_e^2/c^2)$. The relativistic solution is

$$\omega_\delta = \mathbf{v}_e \cdot \mathbf{k}_\delta - \frac{\hbar}{2\gamma_e m_e}\left(k_\delta^2 - \frac{\omega_\delta^2}{c^2}\right), \tag{4.16}$$

from which we can recover the non-relativistic equation by setting $\gamma_e \to 1$ and seeking the solution with $k_\delta^2 \approx \frac{\omega_\delta^2}{u^2} \gg \frac{\omega_\delta^2}{c^2}$.

5 Velocity-space tomography and model fitting

The previous section showed that the principles of energy and momentum conservation suggest that the CTS, FIDA, GRS and NES observe broad regions in velocity space, so that the determination of fast-ion energy spectra from the measurements directly is not possible. Some one-step GRS reactions have direct energy resolution [7], but unfortunately they do not involve α-particles. Further, the diagnostics observe restricted parts of velocity space, so that the direct determination of fast-ion densities is not possible, either. Nevertheless, these important parameters can still be determined by various analysis techniques.

Ideally, the interrogation regions of individual diagnostics can be combined to get a full coverage of the fast-ion phase-space. Integrated data analysis of several diagnostics by velocity-space tomography allows the determination of the 2D velocity distribution function. The integral
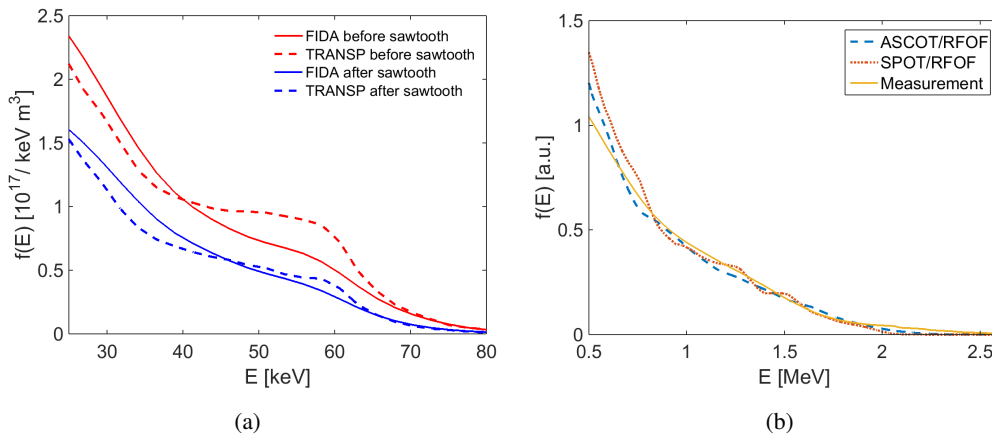
Figure 2. Measurements of fast-ion energy spectra and corresponding simulations. The measurements are obtained by velocity-space tomography and integration over the pitch. (a) FIDA measurement and TRANSP simulation of a fast-ion energy spectrum before and after a sawtooth crash in ASDEX Upgrade discharge #32323 [22]. (b) Combined GRS and NES measurements of an energy spectrum of deuterium ions accelerated by 3rd harmonic ICRF in JET discharge #86459 [23]. The measurements are compared to ASCOT/RFOF and SPOT/RFOF simulations.

over pitch is the energy spectrum [20] and the double integral over energy and pitch gives us the fast-ion density [18, 22]. As the velocity-space tomography problem is ill-posed, we must regularize the solution by prior information. A popular approach is to assume the velocity distribution function to be smooth. As compared to other techniques discussed below, this approach uses the least amount of prior information but requires many measurements.

Energy spectra determined from FIDA measurements in this way appear in figure 2(a) along with a corresponding TRANSP simulation. At ASDEX Upgrade, five FIDA spectra can be acquired simultaneously [20]. The energy spectra show the distribution of core fast-ion energies in ASDEX Upgrade discharge #32323 just before and after a sawtooth crash. A velocity-space tomography movie of this event has been published previously [22]. Here we focus on energy spectra. The neutral beam deuterium injection energy is 60 keV so that the energy spectra are expected to have kinks at 60 keV and 30 keV (half injection energy). The inversions from FIDA measurements show weaker kinks at these energies than the TRANSP simulation. This is expected since the measured 2D velocity distribution functions have smaller beam injection peaks than the TRANSP simulations which is explained by the first-order Tikhonov regularization [22].

Figure 2(b) shows measured energy spectra of fast deuterium ions accelerated by 3rd harmonic ICRF heating at JET as compared to ASCOT/RFOR and SPOT/RFOF simulations [31, 32]. A high-resolution GRS detector and three NES detectors acquired spectra simultaneously [33]. Velocity-space tomography based on the GRS and NES measurements gives a 2D velocity distribution function, from which we obtain the energy spectra by integration over pitch. The agreement between theory and experiment is excellent.

Several important points are lost when considering just the energy spectra, which constitute the α-particle ITER measurement requirement [1], instead of 2D velocity distribution functions. Firstly, the strong anisotropy of the 2D velocity distribution function of the NBI ions is lost due to the

integration over pitch. Secondly, the measured and simulated energy distributions are monotonic whereas the measured and simulated 2D velocity distribution functions have peaks at the full and half injection energy such that a bump-on-tail is formed in 2D velocity space. Nevertheless, energy spectra provide an intuitive meeting ground between theory and experiment. The rich information can further be simplified by integration over the energy to obtain the fast-ion density. The agreement of simulated and measured fast-ion densities determined by this approach is good [7, 18].

At ITER, velocity-space tomography should be possible for α-particle energies $E_\alpha > 1.7$ MeV [28]. A reconstruction of an energy spectrum computed from synthetic GRS and CTS measurements at ITER [34–36] appears in figure 3. The α-particle energy spectrum can be reconstructed by integrated data analysis of the GRS and CTS measurements. We stress again that any velocity-space anisotropy of the α-particle distribution function is not reflected in the energy spectra. To study anisotropy, the full 2D distribution function must be measured but this requires an additional detector with an oblique line-of-sight with respect to the magnetic field [28].
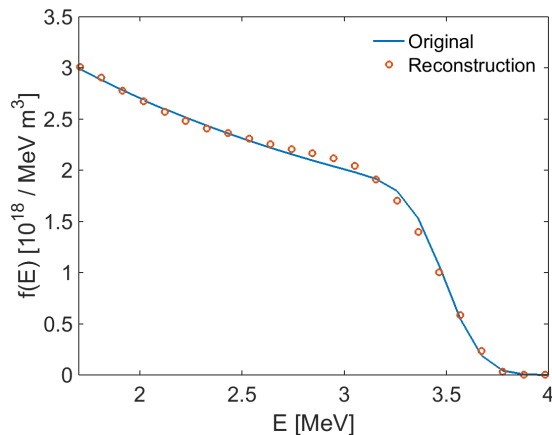

Figure 3. Reconstruction of the energy spectrum for $E > 1.7$ MeV for an isotropic α-particle slowing-down distribution based on synthetic GRS and CTS measurements.

For 0.5 MeV $< E_\alpha < 1.7$ MeV, CTS will be the only direct diagnostic for confined α-particles at ITER since GRS is not sensitive below 1.7 MeV. The lower energy limit arises from the assessment where CTS due to α-particles significantly exceeds CTS due to thermal deuterium and tritium. Depending on assumptions, energies down to about 0.3-0.4 MeV might be accessible. Despite the absence of other diagnostics entering an integrated data analysis, α-particle energy spectra and densities can still be determined using CTS spectra only. To do this we here assume the distribution function to be smooth and isotropic in velocity space. An example of this technique appears in figure 4(a). In particular the region below 1.7 MeV, where GRS is not sensitive, is well reconstructed from the CTS measurements. However, the kink near the α-particle birth energy is not as well reconstructed as is possible in the 2D inversion based on GRS and CTS. The same approach works for single-detector GRS measurements at ITER (figure 4(b)). The GRS inversion does an excellent job at reconstructing the α-particle birth energy due to the very good sensitivity at high energies but GRS becomes insensitive for energies below 1.7 MeV.

A disadvantage of this technique is that the assumption of isotropy precludes the measurement
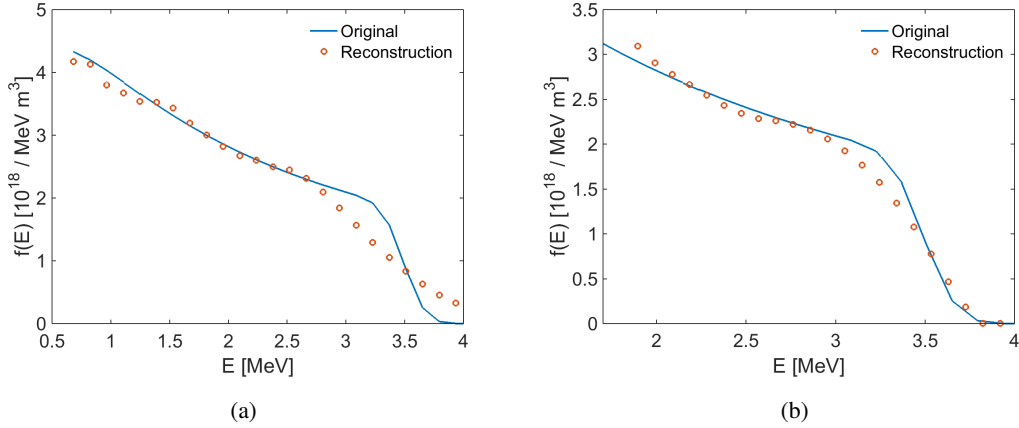
Figure 4. (a) Reconstruction of the energy spectrum for $E > 0.5$ MeV for an isotropic α-particle slowing-down distribution based on single-detector CTS measurements and the prior information that the distribution function is isotropic. (b) As (a), but for GRS for $E > 1.7$ MeV.

of any anisotropy effects. Nevertheless, the ITER measurement requirement to measure α-particle energy spectra can be met down to 0.5 MeV (optimistically 0.3 MeV) based on the CTS measurements. The assumption of isotropy is perhaps already implied by the requirement to measure energy spectra which ignores any pitch effects. This approach allows the determination of the α-particle density under the assumptions that the α-particle velocity distribution function is smooth and isotropic in velocity space. While smoothness is probably a good assumption, the isotropy assumption is questionable since some anisotropy is expected due to the drift orbit topology, the directional bias of NBI and any anomalous transport due to Alfvénic or other magnetohydrodynamic activity [28].

The last approach that we discuss is to fit a model to the measured spectra by assuming a functional form of the α-particle velocity distribution function, for example a classical slowing-down distribution. The assumption of a functional form of the velocity distribution function is stronger prior information yet than isotropy and smoothness. The slowing-down distribution is both isotropic and smooth, and additionally the spectral shape is given (assuming we know the crossover energy). This approach precludes the measurement of energy spectra as they are assumed in the approach. Nevertheless, the α-particle densities can be inferred by determining the α-particle density that produces the best fit to the measured spectra, for example using a least-square metric accounting for nuisance parameters [37]. Figure 5 illustrates the sensitivity of CTS measurements to the α-particle density for an isotropic slowing-down distribution in a deuterium-tritium plasma. The frequency of the injected electromagnetic waves is 60 GHz. The shapes of the measured spectra depend on the α-particle densities which can hence be determined. In particular the wings of the spectra with Doppler shifts larger than about 1 GHz vary strongly with the α-particle density. The inner part of the spectra with Doppler shifts smaller than about 1 GHz are dominated by scattering from thermal deuterium and tritium. Since the isotropic slowing-down distribution is probably a fairly good model, it should allow the determination of α-particle densities with good accuracy.
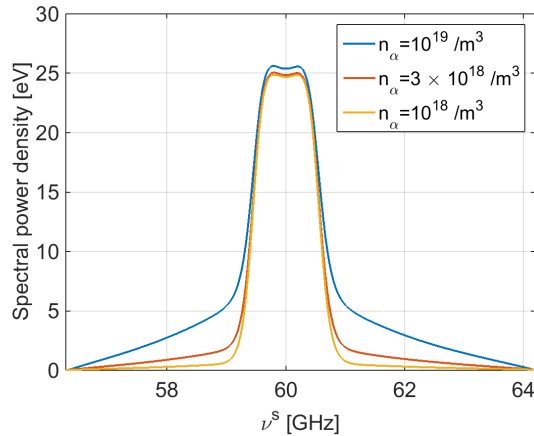
Figure 5. Sensitivity of CTS spectra to the α-particle density for the central CTS measurement volume for the ITER baseline scenario. The α-particle velocity distribution is assumed to be an isotropic slowing-down distribution. The alpha particle density n_α can be inferred by finding the best fit of the model to the measurements.

6   Conclusions

Energy and momentum conservation imply that fast-ion diagnostics observe restricted yet rather broad regions in velocity space. This makes it impossible to directly measure densities and energy spectra of fusion α-particles. The consistent use of energy and momentum conservation stresses the analogies and differences in the velocity-space interrogation regions of NES, GRS, CTS and FIDA. We can nevertheless determine energy spectra and fast-ion densities. Integrated data analysis of the available fast-ion diagnostics allows the tomographic reconstruction of a 2D velocity distribution function which can be integrated to obtain energy spectra and densities. Energy spectra measured in this way at JET and ASDEX Upgrade agree very well with corresponding numerical simulations. This approach will be possible at ITER for α-particles with energies larger than 1.7 MeV based on GRS and CTS. For lower energies down to about 300-500 keV the measurement relies on CTS only, and we need to assume additional prior information on the distribution function to obtain solutions. Energy spectra and densities of the α-particles can be obtained by assuming that their distribution is isotropic in velocity space. Alternatively, fast-ion densities can also be obtained by assuming a functional form of the fast-ion velocity distribution function, such as an isotropic slowing-down distribution, which is stronger prior information yet than smoothness and isotropy.

References

[1] Donné A J H *et al* Progress in the ITER Physics Basis Chapter 7: Diagnostics 2007 *Nucl. Fusion* **47** S337–S384

[2] Heidbrink W W *et al* 2007 *Plasma Phys. Control. Fusion* **49** 1457–1475

[3] Salewski M *et al* 2011 *Nucl. Fusion* **51** 083014

[4] Salewski M *et al* 2014 *Plasma Phys. Control. Fusion* **56** 105005

[5] Jacobsen A S *et al* 2015 *Nucl. Fusion* **55** 053013

[6] Salewski M *et al* 2015 *Nucl. Fusion* **55** 093029

[7] Salewski M *et al* 2016 *Nucl. Fusion* **56** 046009

[8] Jacobsen A S *et al* 2017 *Rev. Sci. Instrum.* **88** 073506

[9] Stagner L and Heidbrink W 2017 *Phys. Plasmas* **24** 092505

[10] Galdon-Quiroga J *et al* 2018 *Plasma Phys. Control. Fusion* **60** 105005

[11] Salewski M *et al* 2018 *Fusion Sci. Tech.* **74** 23–36

[12] Moseev D *et al* 2018 *Rev. Mod. Plasma Phys.* **2** at press

[13] Nocente M *et al* 2015 *Nucl. Fusion* **55** 123009

[14] Salewski M *et al* 2012 *Nucl. Fusion* **52** 103008

[15] Salewski M *et al* 2013 *Nucl. Fusion* **53** 063019

[16] Salewski M *et al* 2014 *Nucl. Fusion* **54** 023005

[17] Salewski M *et al* 2015 *Plasma Phys. Control. Fusion* **57** 014021

[18] Geiger B *et al* 2015 *Nucl. Fusion* **55** 083001

[19] Jacobsen A S *et al* 2016 *Plasma Phys. Control. Fusion* **58** 045016

[20] Weiland M *et al* 2016 *Plasma Phys. Control. Fusion* **58** 025012

[21] Rasmussen J *et al* 2016 *Nucl. Fusion* **56** 112014

[22] Salewski M *et al* 2016 *Nucl. Fusion* **56** 106024

[23] Salewski M *et al* 2017 *Nucl. Fusion* **57** 056001

[24] Weiland M *et al* 2017 *Nucl. Fusion* **57** 116058

[25] Geiger B *et al* 2017 *Plasma Phys. Control. Fusion* **59** 115002

[26] Salewski M *et al* 2018 *Nucl. Fusion* **58** 036017

[27] Madsen B *et al* 2018 *Rev. Sci. Instrum.* **89** 10D125

[28] Salewski M *et al* 2018 *Nucl. Fusion* **58** 096019

[29] Galdon-Quiroga J *et al* 2018 *Phys. Rev. Lett.* **121** 025002

[30] Fermi E 1932 *Rev. Mod. Phys.* **4** 87–132

[31] Schneider M *et al* 2016 *Nucl. Fusion* **56** 112022

[32] Hirvijoki E *et al* 2014 *Comp. Phys. Comm.* **185** 1310–1321

[33] Eriksson J *et al* 2015 *Nucl. Fusion* **55** 123026

[34] Nocente *et al* M 2017 *Nucl. Fusion* **57** 076016

[35] Salewski M *et al* 2009 *Nucl. Fusion* **49** 025006

[36] Salewski M *et al* 2009 *Plasma Phys. Control. Fusion* **51** 035006

[37] Bindslev H 1999 *Rev. Sci. Instrum.* **70** 1093–1099